

Structure of an inert layer of ^4He adsorbed on mesoporous silica

Junko Taniguchi,* Kizashi Mikami, and Masaru Suzuki

Department of Engineering Science, University of Electro-Communications, Chofu, Tokyo 182-8585, Japan



(Received 8 April 2019; revised manuscript received 17 June 2019; published 3 July 2019)

We have performed the measurements of the vapor pressure and heat capacity for inert layer ^4He adsorbed on a mesoporous silica. The heat capacity was found to exhibit a Schottky peak, indicating the excitation of the localized solid to fluid. We analyzed the heat capacity over a wide temperature range according to a model that considers the contribution of the localized solid and excited fluid, and clarified that the excited fluid coexists with the localized solid at high temperatures. Based on the areal density dependence of the amount of excited fluid, we discuss the formation of an inert layer prior to the appearance of a superfluid layer.

DOI: [10.1103/PhysRevB.100.024103](https://doi.org/10.1103/PhysRevB.100.024103)

I. INTRODUCTION

Since the observation of the Kosterlitz-Thouless transition in a ^4He film formed on vycor glass [1], a considerable amount of work has been reported on the structure of ^4He films adsorbed on various substrates. On graphite, which exhibits a homogeneous adsorption potential, layer-by-layer growth of films was confirmed up to six atomic layers [2], and highly complicated phase diagrams have been obtained for the first and second layers [3,4]. Such complicated phase diagrams have not been reported for other substrates because of their heterogeneous adsorption potential. On these substrates, it is thought that an inert layer is formed at areal densities below the value at which a superfluid layer appears (n_C).

Among various heterogeneous substrates, the film structure on a porous vycor glass has been thoroughly studied on the basis of heat capacity measurements [5]. Tait and Reppy attributed the observed bend in heat capacity to the excitation of a part of ^4He from localized solid islands to delocalized gas areas. They reported that, on the high temperature side of the bend, the excited gas coexists with solid islands and covers only a fraction of the total surface area, owing to the lateral pressure caused by the long-range variation of adsorption potential.

Recently, Toda *et al.* studied the film structure of ^4He adsorbed on hybrid mesoporous materials (HMM) based on vapor pressure and heat capacity measurements [6]. They observed a heat capacity similar to that for an inert layer and proposed at areal densities above the value for the completion of the first layer, the heat capacity on the high-temperature side of the bend corresponds to that of a normal fluid with an amorphous-solid-like temperature dependence [7]. In order to confirm this hypothesis, they first qualitatively evaluated the density states of two-level systems (TLSs) in the amorphous solid state using the vapor pressure data.

In the previous work, the structure of the inert layer was discussed on the basis of the heat capacity of limited temperature or areal density regions. In this work, our aim is

to comprehensively and quantitatively study this structure. Thus, we chose the mesoporous silica called folded-sheets-mesoporous materials (FSM), whose adsorption potential has been theoretically studied [8], and performed heat capacity and vapor pressure measurements. We analyzed the heat capacity of the inert layer over a wide temperature range (0.18–4.5 K) according to a model that considers the contribution of localized solid and excited fluid. The results support the conjecture that the excited fluid coexists with the localized solid at high temperatures. On the other hand, the amount of excited fluid tends to zero as the areal density approaches n_C , suggesting a new possibility that the inert layer is solidified at values immediately below n_C .

II. EXPERIMENTS

The synthesis of FSM was first reported by Inagaki *et al.* at Toyota Central R&D Labs., Inc. Japan [9]. This material exhibits a honeycomb structure of straight one-dimensional (1D) uniform nanometer-sized channels without interconnections. Using an organic molecule as a template, the diameter of the channel was precisely controlled, and the homogeneity was confirmed by transmission electron micrography and x-ray diffraction (XRD) [10]. The sample used in this work has channels with a diameter of 2.8 nm and is formed into pellets by mixing it with silver powder.

For heat capacity measurements, we used the cell described in previous heat capacity measurements for pressurized liquid ^4He [11]. The surface area (S) was reduced to 145 m² in the present measurements, by 20% from the previous one [12]. Unlike in the liquid case, the filling capillary is directly connected to the cell since the thermal conductivity is not excessively high.

The heat capacity was measured using a quasiadiabatic heat-pulse technique at up to 14 atoms/nm², which corresponds to the areal density of superfluid onset (n_C) [13]. The temperature of the cell was monitored with RuO₂, which was attached to the bottom face of the cell. This thermometer was calibrated against a calibrated RuO₂ thermometer. The thermal relaxation time from the cell to the stage was

*tany@phys.uec.ac.jp

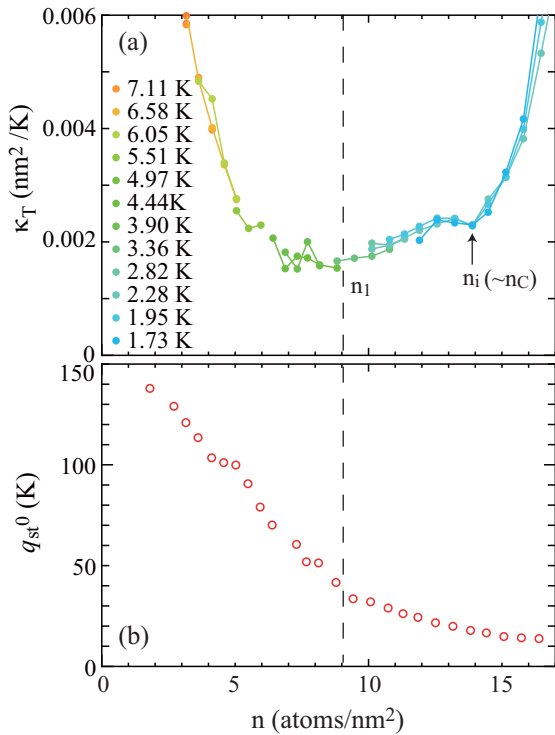


FIG. 1. (a) Two-dimensional isothermal compressibility κ_T and (b) isotheric heat of sorption at absolute zero q_{st}^0 as a function of areal density. The vertical dashed line shows n_1 , while the arrow shows n_i .

360–5000 s, which is more than one order of magnitude larger than that in the cell, 40–240 s.

For vapor pressure measurements, we adopted the cell described in previous double torsional oscillator measurements [14]. As in previous work [15], the pressure was measured by means of the capacitive strain gauge with a 100 μm thick membrane, whose one side was Au sputtered as an electrode. The pressure was calibrated against the ^4He saturated vapor pressure. Its accuracy was 2×10^{-3} mbar. This gauge was attached directly to the cell, which was mounted on the 1 K pot of a refrigerator.

III. RESULTS AND DISCUSSION

A. Isothermal compressibility and isotheric heat of sorption

The vapor pressure (P) of the adsorbed ^4He determines the isothermal compressibility (κ_T) and the isotheric heat of sorption (q_{st}), which are useful for examining the changes in the film structure. Since κ_T decreases as the density increases near layer completion, its minimum is often used to indicate layer completion. κ_T is deduced from the P isotherm as

$$\kappa_T = \frac{1}{n^2 k_B T} \left(\frac{\partial n}{\partial \ln P} \right), \quad (1)$$

where n is the areal density, k_B is Boltzmann constant, and T is the temperature.

Figure 1 shows the obtained κ_T as a function of areal density up to 16.4 atoms/nm², where capillary condensation occurs. κ_T shows a minimum at approximately 9 ± 1 atoms/nm², which we designate as the areal density of

the first layer completion (n_1). For values higher than n_1 , κ_T initially increases with increasing areal density and then decreases at approximately 12.7 ± 0.3 atoms/nm², with a slight minimum at $n_i = 14$ atoms/nm². A similar minimum in κ_T was also reported for ^4He in 4.7- and 2.8-nm channels of FSM series by Ikegami *et al.* [15,16]. Just above the areal density of this slight minimum, a superfluid transition is commonly observed in both the present and the previous work, i.e., n_C almost coincides with n_i . This finding indicates that the inert layer is slightly compressed as the areal density approaches n_C .

From the temperature dependence of the vapor pressure, we calculated q_{st} as

$$q_{st} = -k_B \frac{d \ln P}{d(1/T)}. \quad (2)$$

By subtracting the heat capacity of gas-phase ^4He , we estimate the isotheric heat of sorption at absolute zero, $q_{st}^0 = q_{st} - (5/2)k_B T$, which corresponds to the depth of the adsorption potential [6]. The obtained q_{st}^0 is shown as a function of n in Fig. 1(b). It is ~ 140 K at 1.8 atoms/nm² and decreases monotonously with increasing areal density. It reaches ~ 40 K at n_1 , above around which its decrease becomes slow. The obtained value of q_{st}^0 is close to that of 4.7-nm channels of FSM, up to n_1 [15]. This result indicates that the difference in the channel size between 2.8 and 4.7 nm does not strongly affect the adsorption potential in the submonolayer region.

B. Heat capacity of inert layer ^4He

Figure 2 shows the heat capacity (C) for various areal densities as a function of T . Here the heat capacity of the empty cell is subtracted. Its magnitude is around half of the one of ^4He at 3.5 atoms/nm² above 1 K, while it becomes comparable near the lowest temperature. For 3.5 atoms/nm², a broad peak appears at around 1.1 K, in addition to the slope slightly smaller than T^2 . With increasing areal density, this peak shifts to the low-temperature side, with its height decreasing. Finally, it becomes unclear above 11.4 atoms/nm². Since the peak is very broad, we define T_p as the temperature at which C/T begins to deviate from the extrapolation of the low-temperature side, which gives the lower limit of the peak temperature (see the inset of Fig. 2). In contrast, the temperature dependence on the high-temperature side remains below T^2 up to around 10.2 atoms/nm², and above that the slope decreases slightly.

As shown in the inset of Fig. 2, the heat capacity above T_p can be explained by the sum of the T -linear (y -intercept) and T -squared (slope) terms. In addition, there is a peak near T_p . Notably, the heat capacity near the lowest temperature is lower than the extrapolated value from the high-temperature side of T_p (dashed line in the inset of Fig. 2). The difference for the T -linear term may stem from the contribution of the excited atoms near T_p .

We set the heat capacity model as

$$C = (A_1 T + B T^2) + C_f + D \frac{(\beta \Delta E)^2}{\cosh^2(\beta \Delta E)}, \quad (3)$$

$$C_f = A_f \frac{\exp(-\beta \Delta E)}{\exp(\beta \Delta E) + \exp(-\beta \Delta E)} T, \quad (4)$$

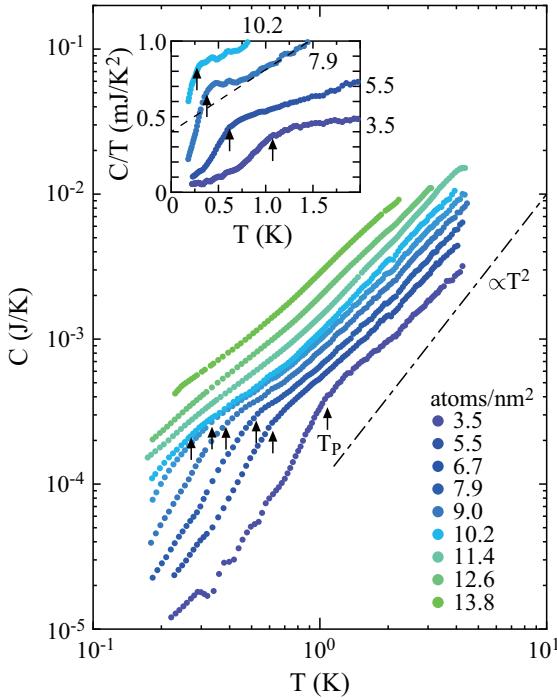


FIG. 2. Heat capacity of ^4He as a function of temperature for various areal densities below 14 atoms/nm^2 . The arrows indicate T_p , and the dot-dashed line is proportional to T^2 . The areal densities are presented in units of atoms/nm^2 . Inset: C/T as a function of T below 10.2 atoms/nm^2 . The dashed line displays an extrapolation from the high-temperature side of the peak.

where $\beta = 1/k_B T$. Here, the first set of parentheses, the second and third terms correspond to the heat capacity of the localized solid, the two-dimensional (2D) excited-fluid ^4He , and a Schottky peak due to the excitation, respectively. Regarding their origins, Tait and Reppy suggested that the $A_1 T$ and the BT^2 terms arise from the amorphous property and 2D phonon of the localized solid and that C_f from the Bose-gas-like behavior of the excited fluid. $A_f T$ means the heat capacity of the excited fluid at temperatures much higher than T_p , and $2\Delta E$ is the energy gap between the localized solid and the 2D fluid states. On the basis of this model, we will evaluate the film structure.

Figure 3(a) shows the fitted curves for 5.5 atoms/nm^2 as an example. The heat capacity is well reproduced over the entire temperature range. Near the lowest temperature, the $A_1 T$ term becomes dominant, whereas near the highest temperature the BT^2 term is dominant. At around T_p , the contribution of the Schottky peak increases, and the coefficient of the T -linear term increases because of the contribution of C_f . As the areal density is increased, the contribution of the Schottky peak and C_f decreases, as is clear from the heat capacity at 9.0 atoms/nm^2 in Fig. 3(b). Further increasing areal density, their contribution disappears, as shown in Fig. 3(c) (13.8 atoms/nm^2). The heat capacity for all areal densities between 3.5 and 13.8 atoms/nm^2 is fitted well to Eq. (3).

C. Properties of the localized solid

It is well known that the amorphous property of the localized solid is characterized by the T -linear heat capacity due

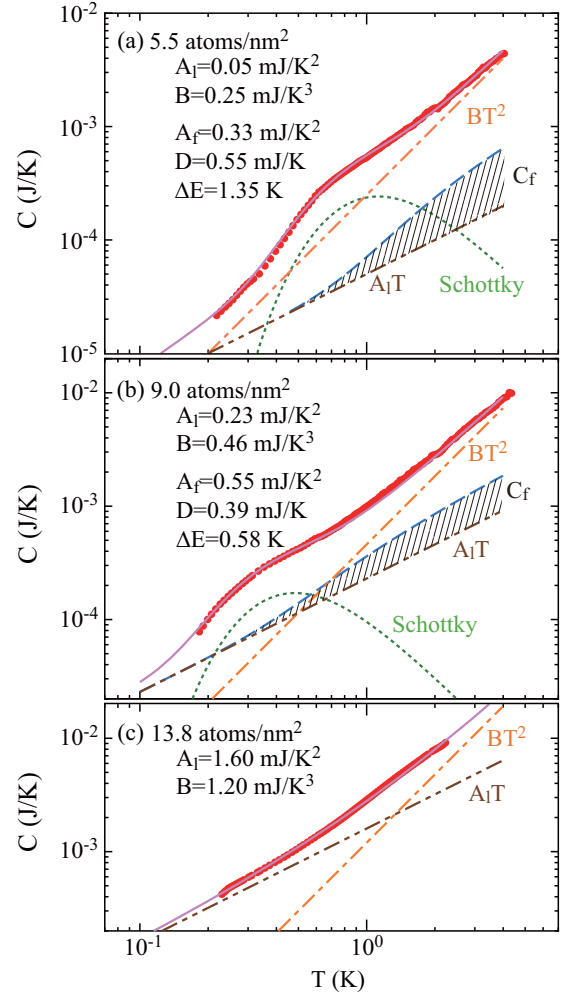


FIG. 3. Heat capacity of ^4He at (a) 5.5 , (b) 9.0 , (c) 13.8 atoms/nm^2 as a function of temperature. The solid curves are the fitted curves to Eq. (3). The dot-dot-dashed, dot-dashed, and dotted curves correspond to the $A_1 T$, BT^2 , and the Schottky terms in Eq. (3), respectively. The hatched areas correspond to C_f .

to quantum tunneling between different states in the two-level systems (TLSs). Figure 4(a) shows the fitting results for A_1 as a function of areal density. The values remain small until approximately 9 atoms/nm^2 and then increase rapidly with increasing areal density.

The coefficient of the T -linear heat capacity for the amorphous solid is described as $A_{AS} = \pi^2/6 \cdot D_0 k_B$, where D_0 is the density of states [6]. When the TLS is generated by the adsorption potential distribution, D_0 is often approximated as [5,6]

$$D_0 = \left(\frac{\Delta q_{st}^0}{\Delta n} \right)^{-1}. \quad (5)$$

Using q_{st}^0 in Fig. 1(b), we estimated A_{AS} , which is shown in Fig. 4(a) for comparison. The calculated A_{AS} shows the same areal density dependence as A_1 , except that the values are slightly larger than A_1 . This semiquantitative agreement indicates that the $A_1 T$ term is well explained by the contribution of amorphous solid.

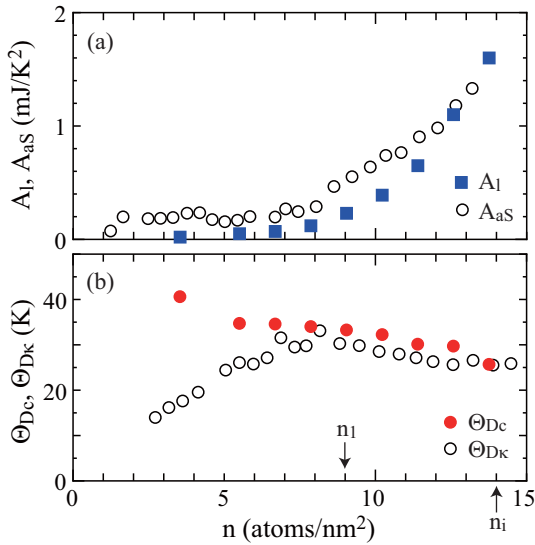


FIG. 4. (a) Fitting results for A_1 and the calculated A_{aS} as a function of areal density. (b) Debye temperatures obtained from B (Θ_{Dc}) and κ_T ($\Theta_{D\kappa}$) as a function of areal density.

Next, we consider the BT^2 term. From the fitting result for B , we calculate the effective Debye temperature Θ_{Dc} as $\Theta_{Dc} = \sqrt{12\zeta(3)\Gamma(3)Nk_B/B} = \sqrt{28.8Nk_B/B}$, where N is the number of solid ^4He atoms. Here, we approximate N by multiplying n by the surface area S , neglecting the number of excited ^4He atoms. The areal density dependence of Θ_{Dc} is shown in Fig. 4(b). Θ_{Dc} is 43 K for 3.5 atoms/nm² and decreases to ~ 35 K at 5.5 atoms/nm², and for higher densities decreases slightly with increasing areal density. The value at around n_1 (34 K) is close to those of other substrates such as Ar-plated Cu (32 K) [17] and graphite (33 K) [18].

The Debye temperature can also be deduced from the phonon velocity (v_p) as $\Theta_{D\kappa} = (hv_p/k_B)\sqrt{n/\pi}$. The phonon velocity is related to the adiabatic compressibility κ_S as $v_p = \sqrt{1/(m\kappa_S)}$. Here, we evaluate $\Theta_{D\kappa}$ by assuming that κ_T is approximately equal to κ_S [6]. $\Theta_{D\kappa}$ increases with increasing areal density and then begins to decrease at 8 atoms/nm², above which $\Theta_{D\kappa}$ agrees well with Θ_{Dc} . It remains unclear why $\Theta_{D\kappa}$ is smaller than Θ_{Dc} below 8 atoms/nm². However, it is possible that, in this areal density region, the solid islands are considered to be independent of each other. In this situation, κ_T may not reflect the compressibility of the solid ^4He itself.

The monotonic decrease of Θ_{Dc} with increasing areal density is not intuitive. Naively, when the areal density increases, the film is expected to be compressed, making the film stiff (i.e., raising the Debye temperature). In fact, for monolayer ^4He adsorbed on graphite, an increase in the Debye temperature has been reported [18]. In order to understand the monotonic decrease of Θ_{Dc} , it is necessary to consider the fact that the local areal density is not uniform on heterogeneous substrates.

D. Excitation to the 2D fluid state

First, we focus on the Schottky peak. In Figs. 5(a) and 5(b), ΔE , and D divided by $k_B S$ are plotted as a function

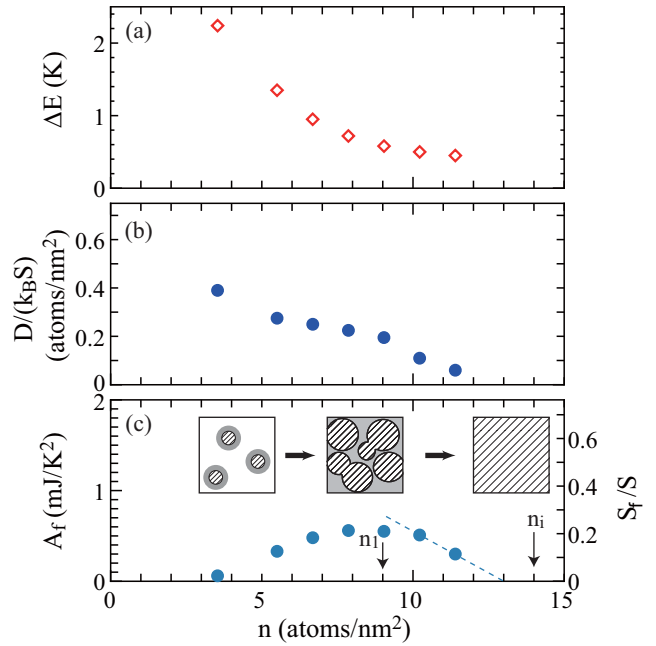


FIG. 5. Fitting results for (a) ΔE , (b) $D/(k_B S)$, and (c) A_f as a function of areal density. In (c), the dashed line shows the extrapolation of the decrease above 10 atoms/nm². The right vertical axis of (c) is S_f/S . The inset plots in (c) show schematic top views of the film at approximately 3.5 atoms/nm², n_1 , and n_i , from left to right (at $T \gg T_p$ for the former two areal densities). The hatched and gray areas correspond to solid and fluid areas, respectively.

of n , respectively, for values up to 11.4 atoms/nm², above which a peak cannot be identified. Here, $D/(k_B S)$ corresponds to the number of atoms that can be excited per unit of areal density. ΔE is 2.2 K for 3.5 atoms/nm² and decreases with increasing areal density, at a decreasing rate. The areal density dependence and the order of magnitude of ΔE agree with those for ^4He on vycor glass, supporting the view that the adsorbed ^4He on the present substrate is excited to the fluid state.

On the other hand, $D/(k_B S)$ is at most $\sim 10\%$ for 3.5 atoms/nm² and decreases with increasing areal density. Above n_1 , it decreases at an accelerated rate and appears to reach zero at approximately 13 atoms/nm². The fitting results indicate that the 2D fluid disappears immediately before n_i .

In order to examine the relation between the amount of 2D fluid ^4He and the magnitude of the T -linear heat capacity, we plot A_f as a function of n in Fig. 5(c). A_f is 0.06 mJ/K² for 3.5 atoms/nm² and initially increases with increasing areal density. It remains almost constant between 8 and 10 atoms/nm² and then decreases. It is important that A_f is not proportional to $D/k_B S$ [i.e., the amount (areal density) of 2D fluid at high temperatures].

In the case where the excited fluid behaves as an ideal 2D Bose gas, the heat capacity is T linear and depends not on the areal density of the fluid but on the surface area that the fluid covers (S_f). The coefficient is expressed by $(mS_f)/(2\pi\hbar^2) \cdot k_B^2$, where m is the mass of the ^4He atom [19]. When the entire surface area is covered, the coefficient reaches 2.6 mJ/K², which is much larger than the obtained A_f , suggesting

that only a part of the surface is occupied by the excited fluid.

Based on the change in S_f/S , we consider the structure of the inert layer. Here, we define S_f/S as $A_f/(2.6 \text{ mJ/K}^2)$, which is shown as the right vertical axis of Fig. 5(c). On the other hand, the surface area covered by the localized solid (S_s) increases roughly in proportion to n/n_1 , in the submonolayer region. S_f initially increases in conjunction with n and its increase stops at approximately 8 atoms/nm², where the sum of S_f and S_s exceeds S . The almost constant S_f from 8 to 10 atoms/nm² indicates that the ratio of localized solid in the first layer increases, while the location of the excited fluid shifts to the overlayer. This trend is thought to be accompanied by the compression of the first layer, since κ_T reaches a minimum in the same areal density region. At higher areal densities, S_f/S begins to decrease and tends to zero at approximately 13 atoms/nm². This behavior is attributed to the increased density in the overlayer, which increases the ratio of solid to fluid in the overlayer and finally enables the solidification of the entire overlayer. This trend is consistent with the decrease in κ_T above approximately 13 atoms/nm², demonstrating that the compression starts at the end of the coexistence of the fluid and solid.

As the origin of the limit for S_f , the lateral pressure due to the long-range variation of adsorption potential is suggested [5]. In the case of porous vycor glass, it is thought that the pore size distribution determines the variation of adsorption potential. Although the channel size of FSM is uniform, it has been reported that the adsorption potential of a hexagonal channel has an azimuthal dependence on the cross section [8]. Its amplitude is several tens of Kelvins near the pore wall and decreases as the distance from the wall increases [i.e., as the film thickness (areal density) increases]. The amplitude of variation of the adsorption potential in the submonolayer region is larger than the obtained ΔE , allowing the excited fluid to localize only around the boundaries of the solid islands.

E. Phase diagram

Here, we evaluate the phase diagram of ^4He film on the bases of the foregoing discussion. Figure 6 presents T_p and the dissipation peak temperature due to the superfluid in the channel (T_C), as a function of areal density. In the low areal density region, ^4He atoms are adsorbed onto areas with a deep adsorption potential and form solid islands at low temperatures. Near T_p , a small part of the localized solid is excited and forms a fluid area surrounding the solid islands. With increasing areal density, T_p decreases because of the decrease in the variation of adsorption potential and finally reaches zero at approximately 13 atoms/nm². Above this areal density, instead of a decrease in the fluid areas, we observe a compression of the inert layer composed of only solid. Then above n_i , a liquid layer which shows superfluidity below T_C appears on top of the inert layer.

This phase diagram is similar to the characteristic diagram of adsorbed ^4He on porous vycor glass proposed by Tait and

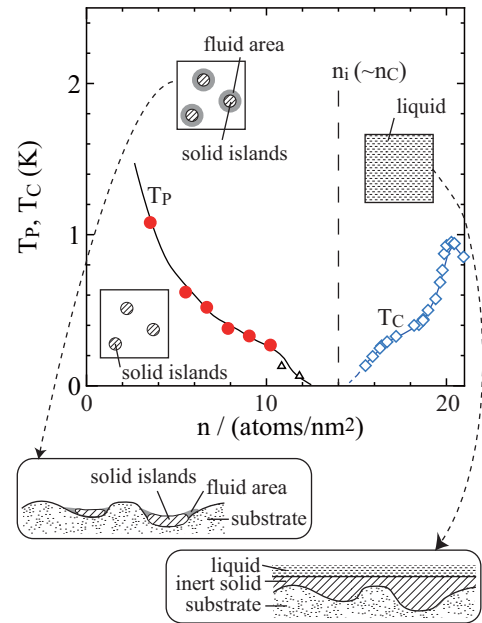


FIG. 6. T_p and the dissipation peak temperature due to the superfluid in the channel (T_C) as a function of areal density. The triangles (Δ) presents T_p from Ref. [20]. The dashed line corresponds to n_i , which coincides with n_c experimentally. Inset: Schematic top views of the film near the lowest temperature and slightly above T_p at $n < n_i$, and above T_C at $n > n_i$, from left to right. The two lower left and right panels show cross-sectional images of the films slightly above T_p and above T_C , respectively.

Reppy [5]. The only difference is that the fluid and liquid phases are separated by the solidification at immediately below n_i . We consider that, after the inert layer is completed and the lateral pressure becomes significantly small, the uniform 2D liquid phase appears. This hypothesis is consistent with the fact that the superfluid fraction is almost proportional to $(n - n_i)$.

IV. SUMMARY

In summary, we studied the structure of inert-layer ^4He in a 2.8-nm channel of FSM, on the bases of vapor pressure and heat capacity data. We also analyzed the heat capacity of the inert layer according to a model that considers the contribution of localized solid and excited fluid. The results support the viewpoint that the excited fluid coexists with the localized solid at high temperatures. With increasing areal density, the amount of excited fluid decreases and tends to zero just below n_i ($\sim n_c$), suggesting that the inert layer is solidified at values slightly below n_i .

ACKNOWLEDGMENTS

The work was partially supported by JSPS KAKENHI Grants No. JP26400352 and No. JP18K03535. We thank S. Inagaki for supplying FSM.

- [1] D. J. Bishop and J. D. Reppy, *Phys. Rev. Lett.* **40**, 1727 (1978).
- [2] G. Zimmerli, G. Mistura, and M. H. W. Chan, *Phys. Rev. Lett.* **68**, 60 (1992).
- [3] M. Shick, in *Phase Transitions in Surface Films*, edited by J. G. Dash and J. Ruvalds (Plenum, New York, 1980).
- [4] D. S. Greywall and P. A. Busch, *Phys. Rev. Lett.* **67**, 3535 (1991); D. S. Greywall, *Phys. Rev. B* **47**, 309 (1993).
- [5] R. H. Tait and J. D. Reppy, *Phys. Rev. B* **20**, 997 (1979).
- [6] R. Toda, M. Hieda, T. Matsusita, and N. Wada, *J. Phys.: Conf. Ser.* **150**, 032112 (2009).
- [7] A. F. Andreev, *Pis'ma Zh. Éksp. Teor. Fiz.* **28**, 603 (1978) [*JETP Lett.* **28**, 556 (1978)].
- [8] M. Rossi, D. E. Galli, and L. Reatto, *J. Low Temp. Phys.* **146**, 95 (2007).
- [9] S. Inagaki, Y. Fukushima, and K. Kuroda, *J. Chem. Soc. Chem. Commun.* **22**, 680 (1993).
- [10] S. Inagaki, A. Koiwai, N. Suzuki, Y. Fukushima, and K. Kuroda, *Bull. Chem. Soc. Jpn.* **69**, 1449 (1996).
- [11] J. Taniguchi, R. Fujii, and M. Suzuki, *Phys. Rev. B* **84**, 134511 (2011).
- [12] The nitrogen vapor pressure isotherms taken in the previous [11] and the present heat capacity measurements are scaled by areal density and show a plateau at the same pressure due to the capillary condensation. The fact indicates that although a part of channels are blocked, the remaining channels keep the adsorption property of FSM16. A similar decrease of the surface area was observed after the sintering process of the pellet by mixing Ag powder. A creep of Ag powder since the previous measurements may be the origin of blocking the channel.
- [13] K. Demura, J. Taniguchi, and M. Suzuki, *J. Phys. Soc. Jpn.* **86**, 114601 (2017).
- [14] J. Taniguchi, K. Demura, and M. Suzuki, *Phys. Rev. B* **88**, 014502 (2013).
- [15] H. Ikegami, T. Okuno, Y. Yamato, J. Taniguchi, N. Wada, S. Inagaki, and Y. Fukushima, *Phys. Rev. B* **68**, 092501 (2003).
- [16] Although the lot number for the 2.8-nm sample is different in the work of Ikegami *et al.* [15] and the present one, the areal density dependences of κ_T basically agree with each other.
- [17] N. N. Roy and G. D. Halsey, *J. Low Temp. Phys.* **4**, 231 (1971).
- [18] M. Bretz, J. G. Dash, D. C. Hickernell, E. O. McLean, and O. E. Vilches, *Phys. Rev. A* **8**, 1589 (1973).
- [19] J. Daunt, *Phys. Lett. A* **41**, 223 (1972).
- [20] R. Toda, M. Hieda, T. Matsushita, N. Wada, J. Taniguchi, H. Ikegami, S. Inagaki, and Y. Fukushima, *Phys. Rev. Lett.* **99**, 255301 (2007).